Innovative Infrastructure Solutions (2020) 5:57
https://doi.org/10.1007/s41062-020-00301-2

TECHNICAL PAPER

Effect of reclaimed asphalt pavement in granular base layers on predicted pavement performance in Egypt

Eman Mousa[2,3] · Sherif El-Badawy[3] · Abdelhalim Azam[1,3]

Received: 21 January 2020 / Accepted: 6 May 2020 / Published online: 26 May 2020

Abstract

This research presents the prediction of pavement performance constructed with base layer consisting of reclaimed asphalt pavement (RAP)/virgin aggregate blends. The prediction was made by the Multi-Layer Elastic Analysis software (KENLAYER) in terms of horizontal tensile strain at the bottom of AC layer and the vertical resilient strain at critical locations within the pavement system. The dynamic modulus |*E**| for the hot mix asphalt was estimated by using the quality-related specifications software considering three different climatic conditions and two levels of design speeds. Finally, total pavement rutting and fatigue cracking were determined using the critical strains computed by the Multi-Layer Elastic Analysis along with the Mechanistic Empirical Pavement Design Guide performance models and transfer functions. In general, the RAP blends showed superior/comparable performance compared to natural aggregates for the application in base/subbase layers for the Egyptian conditions. The effect of the rate of loading and climate conditions was significant on both asphalt concrete layer fatigue cracking and rutting.

Keywords Reclaimed asphalt pavement (RAP) · QRSS · MEPDG · Performance · Rutting · Fatigue

Introduction

Pavement structures are subjected to different levels of traffic loading with variable speeds and environmental changes that may lead to various distresses. Pavement performance mainly relies on material properties, traffic levels, climate conditions, and construction quality [1]. The mechanical properties of the unbound granular materials (UGMs) are affected by material type and its characteristics along with moisture content variations, which depend on the climate condition.

✉ Abdelhalim Azam
amazam@ju.edu.sa; abdelhalim.azam@mans.edu.eg

Eman Mousa
eman_mosa89@yahoo.com; emousa@horus.edu.eg

Sherif El-Badawy
sbadawy@mans.edu.eg

[1] College of Engineering, Jouf University, Sakakah, Kingdom of Saudi Arabia

[2] Civil Engineering Department, Horus University, Dumyat Al Jadidah 34511, Egypt

[3] Public Works Engineering Department, Mansoura University, Mansoura 35516, Egypt

In recent years, the waste materials have received more attention from researchers and practitioners worldwide. The interest in these materials was necessitated by the population growth, which led to large consumption of natural resources. Thus, the use of recycled materials appeared promising from a wide variety of viewpoints, which increases the awareness to a greener environment. The waste materials include a wide range of excavated materials such as rock, soil, reclaimed asphalt pavement (RAP), bricks, concrete, plastic wastes, scrap tires, foundry sand, oil sand marble dust, and steel slag [2–4]. A great deal of research effort has been performed in this direction, and still there is ongoing research along with field studies for better understanding the behavior of these materials and increasing their utilization. Aside from benefits and encouraging research recommendations and practical results obtained from recycling waste materials as a substitution to natural materials, the lack of actual experience and some environmental issues have delayed the wide applications of such materials [4].

RAP is considered as one of the most recycled materials widely used in pavement construction. It is produced from the milling of the aged asphalt layers during rehabilitation, resurfacing, or pavement reconstruction projects, which increase every day. RAP has several applications, for example as a

granular material in the base or subbase layers in paved and unpaved roadways, gravel roads rehabilitation, shoulders, bicycle paths, driveways, parking areas and as a fill material [5–9]. Extensive laboratory and field studies in the literature were conducted on the evaluation of RAP performance as unbound granular material either blended with virgin aggregate (VA) or alone. Table 1 summarizes different previous literature studies focused on characterizing properties of blends of RAP and virgin aggregates as base/subbase materials. Based on laboratory and/or field testing, these studies reported superior properties of the RAP/VA blends as compared to virgin aggregates. The studies also reported that RAP is a viable and cost-effective base/subbase material if blended with VA. Furthermore, some studies reported that California bearing ratio (CBR) decreases as the RAP amount increases [9, 11, 13, 17, 19, 22, 25]. However, the resilient modulus (M_r) has a opposite trend, which increases with the increase in RAP amount in the blend [5, 7, 9, 11, 12, 14–17, 20, 23, 24]. This is attributed to the binder in the RAP, which leads to better resilient behavior. The reasons for the different behaviors of CBR and M_r with the increase in RAP may be the high load applied during the CBR test, which is a failure test compared to the M_r test that facilitates the sliding of the asphalt-coated aggregates over each other leading to higher deformation. For the M_r, the addition of RAP to virgin aggregate mixes provides some kind of stabilization because of the presence of asphalt coating in the RAP aggregate, which makes the mixture stiffer at the low state of stress during the M_r test. Other studies discussed the performance of treated or untreated RAP/VA blend in terms of CBR, unconfined compressive strength (UCS) and M_r [26, 27].

Few studies are available for the prediction of RAP performance by the Mechanistic Empirical Pavement Design Guide (MEPDG) software. Alam et al. [5] evaluated the effect of RAP amount as subbase (different percentages: 0%, 30%, 50%, 70%, and 100%) on pavement performance. The simulation results indicated that as RAP amount increased in the blend, the predicted fatigue cracking of the AC layer decreased. However, the predicted rutting of the subbase was slightly affected by the RAP content. The difference in rutting was found to be less than 0.05 in. (1.4 mm) between 0 and 100% RAP blends. In a similar study, Schwartz et al. [28] conducted sensitivity analyses of performance predictions to MEPDG design inputs under three traffic volume levels and five climatic conditions. The authors reported that the longitudinal and bottom-up fatigue cracks are very sensitive to the thickness of base material and M_r of both layers of subgrade and base.

Although the laboratory characterization of RAP as a pavement material was well investigated, limited studies are available on the prediction of pavement performance containing recycled products especially RAP as base material and the significance of RAP blends as base/subbase on rutting and fatigue performance. Furthermore, the license of MEPDG is too costly at least for developing countries like Egypt and it requires many inputs that may not be readily available at many agencies.

Research objectives

The main objective of this research is to build a framework for the prediction of field performance of RAP blends by incorporating the KENLAYER and quality-related specifications software (QRSS) along with the MEPDG sophisticated models which consider cost saving. The pavement response will be determined by designed Excel sheets that solve the sophisticated models of MEPDG in a simplified method.

Mechanistic Empirical Pavement Design Guide

The MEPDG is an advanced tool for the design and analysis of both new and rehabilitated flexible pavement structures [29]. It predicts the accumulated damage based on monthly/bimonthly changes of traffic, climate, and consequently construction material properties. After that, damage is converted into expected smoothness and pavement distresses using empirical transfer functions calibrated either globally or locally. For flexible pavements, performance is indicated in terms of rutting (total pavement rutting and individual layer rutting), top-down longitudinal cracking, bottom-up fatigue cracking and transverse (thermal) cracking [29].

MEPDG has three different hierarchical levels of inputs regarding traffic, materials, and environmental conditions. For material inputs, level 1 possesses the highest accuracy and reliability level and lowest error as the input values are obtained from direct laboratory measurements. In level 2, the input data are based on correlations with routine engineering tests to calculate material properties. Finally, default values based on experience are used as inputs for level 3 [29].

MEPDG distress prediction models

The most important pavement structural distresses are rutting, bottom-up fatigue cracking. In the following sections, MEPDG rutting and fatigue cracking models are detailed.

Rutting models

Total rutting is the summation of the permanent deformation of each layer of the pavement structure (i.e. hot mix asphalt, HMA layers, unbound layers, and subgrade soil). Table 2 displays the models (Eqs. 1–3) used in MEPDG for HMA rutting calculations [29]. Equations (4) and (5) depict the models for

Table 1 Summary of previous studies of RAP blends with virgin aggregate

References	RAP/aggregate blends	Testing	Most important results
Sayed et al. [10]	0/100, 100/0	Gradation–Compaction–LBR[1] *Lime bearing ratio (LBR)–falling weight deflectometer (FWD)*	Untreated RAP as base in paved shoulders construction was found to be an economically and technically feasible alternative to traditional lime rock
Garg and Thompson [11]	0/100, 100/0	Gradation–compaction–M_r–rapid shear–permanent deformation *FWD–dynamic cone penetrometer (DCP)*	RAP can be successfully used as conventional flexible pavement base material
Papp et al. [12]	0/100, 25/75, 50/50, 75/25, 100/0	Gradation–compaction–M_r	RAP is a viable alternative as pavement base/subbase layer and cost-effective material for pavement construction
Taha et al. [13]	0/100, 20/80, 40/60, 60/40, 80/20, 100/0	Gradation–compaction–CBR	Up to 60% RAP was qualified for use in road subbase in Oman. However, only 10% RAP was qualified as a road base construction
MacGregor et al. [14]	0/100, 10/90, 30/70, 50/50, 100/0	Gradation–compaction–permeability–M_r	RAP is considered to be a beneficial substitute to the base and subbase materials
Bejarano [15]	0/100, 100/0	Gradation–compaction–M_r *FWD–DCP*	Evaluation of the recycled material properly indicated the response and performance of the RAP as base material based on the field and laboratory tests
Cosentino et al. [16]	0/100, 60/40, 80/20, 100/0	Gradation–compaction–LBR Permeability–M_r *CBR–FWD–Clegg Impact (CIT)–soil stiffness gauge (SSG)*	80% RAP provided the best strength properties while maintaining a reasonable permeability coefficient
Bennert and Maher [17]	0/100, 25/75, 50/50, 75/25, 100/0	Gradation–compaction–CBR Permeability–M_r	RAP blended with virgin aggregate is limited to 50% for subbase layer
Trzebiatowski and Benson [18]	0/100, 100/0	Gradation–compaction–permeability	RAP should drain as well as or be better than conventional base material
Guthrie et al. [19]	0/100, 25/75, 50/50, 75/25, 100/0	Gradation–compaction–CBR	The use of RAP is environmentally responsible and offers potentially significant cost savings Thicker pavement base layers, base stabilization or both may be required in many instances to ensure adequate long-term pavement performance
Gupta et al. [20]	0/100, 25/75, 50/50, 75/25, 100/0	Gradation–compaction–permeability–M_r	RAP mixtures are good substitutes for virgin aggregates in base and subbase layers of roads
Locander [21]	0/100, 100/0	Gradation–compaction–permeability–M_r	RAP demonstrated similar engineering pavement design properties as unbound aggregate base course. Usage of RAP as an unbound aggregate base course is an appropriate alternative design and construction approach
Alam et al. [5]	0/100, 30/70, 50/50, 70/30, 100/0	Gradation–compaction–M_r	RAP is a viable alternative as a base layer by means of fundamental engineering properties
Wu [7]	0/100, 20/80, 40/60, 60/40, 80/20	Gradation–compaction–permeability–X-ray CT–M_r	RAP can be used for granular base

Table 1 (continued)

References	RAP/aggregate blends	Testing	Most important results
Dong and Huang [8]	0/100, 100/0	Gradation–compaction–M_r	No pure unbound RAP base was recommended for asphalt pavements. When such options were to be made, in addition to considering pavement structure and thickness, cautions should be exercised (such as interpreting the resilient modulus, considering the creep and permanent deformation behaviors of the unbound RAP materials)
Luo [14]	0/100, 25/75, 50/50, 75/25, 100/0	Gradation–compaction–CBR–M_r	75% RAP content achieved the highest resilient modulus in aggregate-RAP blends
Stolle et al. [21]	0/100, 12.5/87.5, 25/75, 37.5/62.5, 50/50	Gradation–compaction–CBR–M_r	Certain combinations of RAP and typical Ontario granular material can be made to form granular bases that have strength similar to that of conventional Ontario granular material
Kolay and Singh [9]	0/100, 20/80, 40/60, 60/40, 80/20	Gradation–compaction–CBR–M_r	RAP can be used as a granular base for road pavement works
Mousa [22]	0/100, 20/80, 40/60, 60/40, 80/20, 100/0	Gradation–compaction–CBR–permeability–X-ray CT–M_r	RAP is a viable alternative and cost-effective material as a base/subbase layer for paved and unpaved roads

Testing in italic is field testing

Table 2 MEPDG rutting models [29]

Equation	Equation number
$\Delta_{p\,(HMA)} = 4.424661 \times 10^{-4} \left(C_1 + C_2 D\right) \varepsilon_{r(HMA)} n^{0.4791} T^{1.5606} 0.328196^{D}$ where $\Delta_{p\,(HMA)}$ = rut depth in the HMA layer, in. $\varepsilon_{r(HMA)}$ = vertical resilient strain calculated by the structural response model (Multi-Layer Elastic Analysis, KENLAYER, in this study) at the mid-depth of the HMA layer/sublayer, in/in n = number of axle load repetitions, T = mix or pavement temperature, °F D = depth below the surface, in	(1)
$C_1 = -0.1039\left(H_{HMA}\right)^2 + 2.4868 H_{HMA} - 17.342$ where H_{HMA} = total HMA thickness, in.	(2)
$C_2 = 0.0172\left(H_{HMA}\right)^2 - 1.733 H_{HMA} + 27.428$	(3)
$\Delta_{p\,(soil)} = k_{s1} \varepsilon_v h_{soil} \left(\frac{\left(e^{(\rho)^{\beta}} \times 0.15\right) + \left(e^{\left(\frac{\rho}{10^9}\right)^{\beta}} \times 20\right)}{2} \right) e^{-\left(\frac{\rho}{n}\right)^{\beta}}$ where $\Delta_{p\,(soil)}$ = permanent or plastic deformation for the layer/sublayer, in n = number of axle load applications ε_v = average vertical resilient or elastic strain in layer/sublayer calculated by the structural response model, in/in h_{soil} = thickness of the unbound layer/sublayer, in k_{s1} = global calibration coefficients, which are 1.673 and 1.35 for granular materials and fine-grained materials, respectively	(4)
$\rho = 10^9 \left(\frac{-4.89285}{\left(1 - (10^9)^{\log^{-1}(-0.61119 - 0.017638(W_c))}\right)} \right)^{\frac{1}{\log^{-1}(-0.61119 - 0.017638(W_c))}}$ where W_c = water content, percent	(5)

computing the rut depth in subgrade soil and unbound pavement layers (refer to Table 2).

Alligator fatigue cracking model

Equation (6) is used for calculating N_f (allowable number of load repetitions) that results in fatigue failure (based on the tensile strain at the bottom of AC layer) as presented in Table 3 [29]. The damage ratio (DI) is used to represent the amount of damage. DI is the division of the axle loads actual number by the allowable number of axle loads to fatigue failure (N_f) as displayed in Eq. (8). Finally, the empirical transfer function is used to determine the area of fatigue cracking as displayed in Eq. (9).

Quality-related specifications software (QRSS)

The quality-related specifications software (QRSS) was developed under the NCHRP Project 9-22 [30] by Fugro Consultants, Inc. and Arizona State University (ASU). This

Table 3 MEPDG alligator fatigue cracking model [29]

Equation	Equation number
$N_{f\text{-HMA}} = 0.007566(C_H)\left(10^{\left(4.84\frac{V_{be}}{V_a+V_{be}}-3.3396\right)}\right)\left(\frac{1}{\varepsilon_t}\right)^{3.9492}\left(\frac{1}{E_{HMA}}\right)^{1.281}$	(6)
where $N_{f\text{-HMA}}$ = allowable number of axle load repetitions for fatigue failure ε_t = tensile strain at the bottom of asphalt layer, in/in E_{HMA} = dynamic modulus of the HMA, psi V_{be} = effective asphalt content by volume, percent V_a = percent air voids of the HMA mixture C_H = thickness correction term, dependent on type of cracking	
$C_H = \left(\frac{1}{0.000398+\frac{0.003602}{1+e^{(11.02-3.49H_{HMA})}}}\right)$	(7)
$DI = \sum(\Delta DI)_{j.m.l.p.T} = \sum\left(\frac{n}{N_{f\text{-HMA}}}\right)_{j.m.l.p.T}$	(8)
where n = actual number of axle load applications within a specific time period j = axle load interval m = axle load type (single, tandem, tridem, quad, or special configuration) l = truck type using the truck classification groups included in the MEPDG p = month T = median temperature for the five temperature intervals or quintiles used to subdivide each month, °F	
$FC_{Bottom} = \left(\frac{1}{60}\right)\left(\frac{6000}{1+e^{(-2C_2^*+C_2^*\text{Log}(DI_{Bottom}*100))}}\right)$	(9)
where FC_{Bottom} = area of alligator cracking that initiates at the bottom of the HMA layers, percent of total lane area, DI_{Bottom} = cumulative damage index at the bottom of the HMA layers	
$C_2^* = -2.40874 - 39.748(1+H_{HMA})^{-2.856}$	(10)

software is a simplification of the MEPDG. The QRSS predicts the rutting of HMA layer and fatigue and thermal cracks for any pavement structure based on the dynamic modulus of the HMA which is a function of traffic speed, volumetric properties of HMA, and climatic data. The prediction of the HMA rutting and alligator fatigue cracking in the QRSS methodology is based on the effective dynamic modulus $|E^*|$ of the HMA as the main property characterizing the HMA stiffness. Even though there are many models available in literature for $|E^*|$ prediction of the HMA [31], the QRSS adopted two different models for $|E^*|$ prediction. These models are Witczak NCHRP 1-37A and Witczak NCHRP 1-40D [30]. In this research, the NCHRP (1-37A) model (Eq. 11, Table 4) was selected as it was reported by several studies to yield better predictions compared to the NCHRP (1-40D) model [31–39]. This is particularly true for the traditional mixes using Marshall mix design and the binder penetration grading system, which are still being used in Egypt.

The QRSS relies on the effective E^*, which is based on the effective temperature (T_{eff}). T_{eff} can be defined as the single temperature where an amount of distress would be equivalent to that occurs from the temperature fluctuation throughout the annual cycles of temperature. In QRSS, T_{eff} for rutting prediction is determined by the methodology presented in NCHRP 2011 and shown in Eq. (12), while for fatigue cracking, Eq. (13) is used as provided in Table 4 [30, 40, 41].

The effective asphalt modulus $|E^*|$ is based on the effective temperature and effective frequency. The effective frequency for fatigue cracking depends on the effective depth, traffic speed, and layer modulus as shown in Eq. (14) [40, 41]. The effective depth for rutting prediction can be computed by Eq. (15), whereas for fatigue, it is located at the bottom of the AC layer.

Materials and methodology

The RAP material used in this research was sourced from a wearing AC surface layer of a major road under rehabilitation located in Port Said Governorate, Egypt. The road has a medium traffic levels and was constructed nearly 20 years ago, and the main pavement distress was the asphalt rutting. The RAP was obtained by a cold milling machine. The RAP properties were examined in the laboratory, and the average percentage of bitumen was 5.2% (by total weight of the mix) based on the extraction results [42]. The asphalt mixture aggregate was crushed dolomite with 19 mm nominal maximum size, and the binder was 60/70 penetration grade.

A crushed dolomite virgin aggregate (VA) was supplied from the Ataqa quarry located in Suez governorate, Egypt. This is a typical aggregate type usually used for the base layer construction in Egypt. Table 5 presents the engineering

Table 4 Models used in QRSS

Equation	Equation number
$\log E^* = -1.249937 + 0.029232P_{200} - 0.001767(P_{200})^2 - 0.002841P_4 - 0.058097V_a - 0.802208\frac{V_{beff}}{(V_{beff}+V_a)} + \frac{3.871977-0.0021P_4+0.003958P_{38}-0.000017(P_{38})^2+0.00547P_{34}}{1+e^{-0.603313-(0.31335\log f)-(0.393532\log \eta)}}$	(11)
where E^* = dynamic modulus of asphalt mix, in 105 psi f = loading frequency, in Hz V_a = air voids in the mix, by volume, % V_{beff} = effective bitumen content, by volume, % P_{34} = cumulative % retained on the 3⁄4-inch sieve P_{38} = cumulative % retained on the 3⁄8-inch sieve P_4 = cumulative % retained on the No. 4 sieve P_{200} = % passing the No. 200 sieve	
$T_{eff\text{ - }rutting} = 14.620 - 3.361\ln(f) - 10.940(z) + 1.121(MAAT) + 1.718(\sigma_{MMAT}) - 0.431(Wind) + 0.333(Sunshine) + 0.080(Rain)$	(12)
where $T_{eff\text{ - }rutting}$ = modified Witczak effective temperature for rutting, °F z = critical depth, in f = loading frequency, Hz MAAT = mean annual air temperature, °F σ_{MMAT} = standard deviation of the mean monthly air temperature, °F Rain = annual cumulative rainfall depth, inches Sunshine = mean annual sunshine percentage (%) Wind = mean annual wind speed (mph)	
$T_{eff\text{ - }fatigue} = -13.9551 - 2.3316(f)^{0.5} + 1.0056(MAAT) + 0.8755(\sigma_{MMAT}) - 1.1861(Wind) + 0.5489(Sunshine) + 0.0706(Rain)$	(13)
where $T_{eff\text{ - }fatigue}$ = modified Witczak effective temperature for fatigue, °F	
$f_{eff} = \frac{17.6v}{2z_{eff}+r}$	(14)
where f_{eff} = effective frequency, Hz v = design speed (mph) z_{eff} = effective depth r = tire contact radius (4.886 inch for the standard wheel)	
$z_{eff} = \sum_{i=1}^{n-1}\left(h_i\sqrt[3]{\frac{E_i}{E_{sg}}}\right) + \frac{h_n}{2}\sqrt[3]{\frac{E_i}{E_{sg}}}$	(15)
where n = number of subdivided layers h_i = subdivided layer thickness (inch) E_i = subdivided HMA layer modulus (psi) E_{sg} = subgrade modulus (psi) h_n = last subdivided HMA layer thickness (inch) E_n = last subdivided HMA layer modulus (psi)	

Table 5 Engineering properties of the virgin aggregate and RAP materials

Experimental test	Test standard	100% VA	100% RAP	Specification limits for the base layer[a]
P200, %	AASHTO T 27-99 [43]	6.40	0.90	5–15
Los Angeles Abrasion (LAA), %	AASHTO T 96-99 [44]	25.5	31.6	50 Max.
Liquid limit (LL), %	AASHTO T 89-96 [45]	24.4	–	25 Max.
Plasticity index (PI), %	AASHTO T 90-00 [46]	5.3	NP[b]	6 Max.
Material classification	AASHTO M 145-91 [47]	A-l-a	A-l-a	–
Modified Proctor test	AASHTO T 180-97 [48]			–
Maximum dry density (MDD), g/cm^3		2.245	1.990	
Optimum moisture content (OMC), %		7.5	6.0	–

[a]According to ECP-104 [49]

[b]Nonplastic

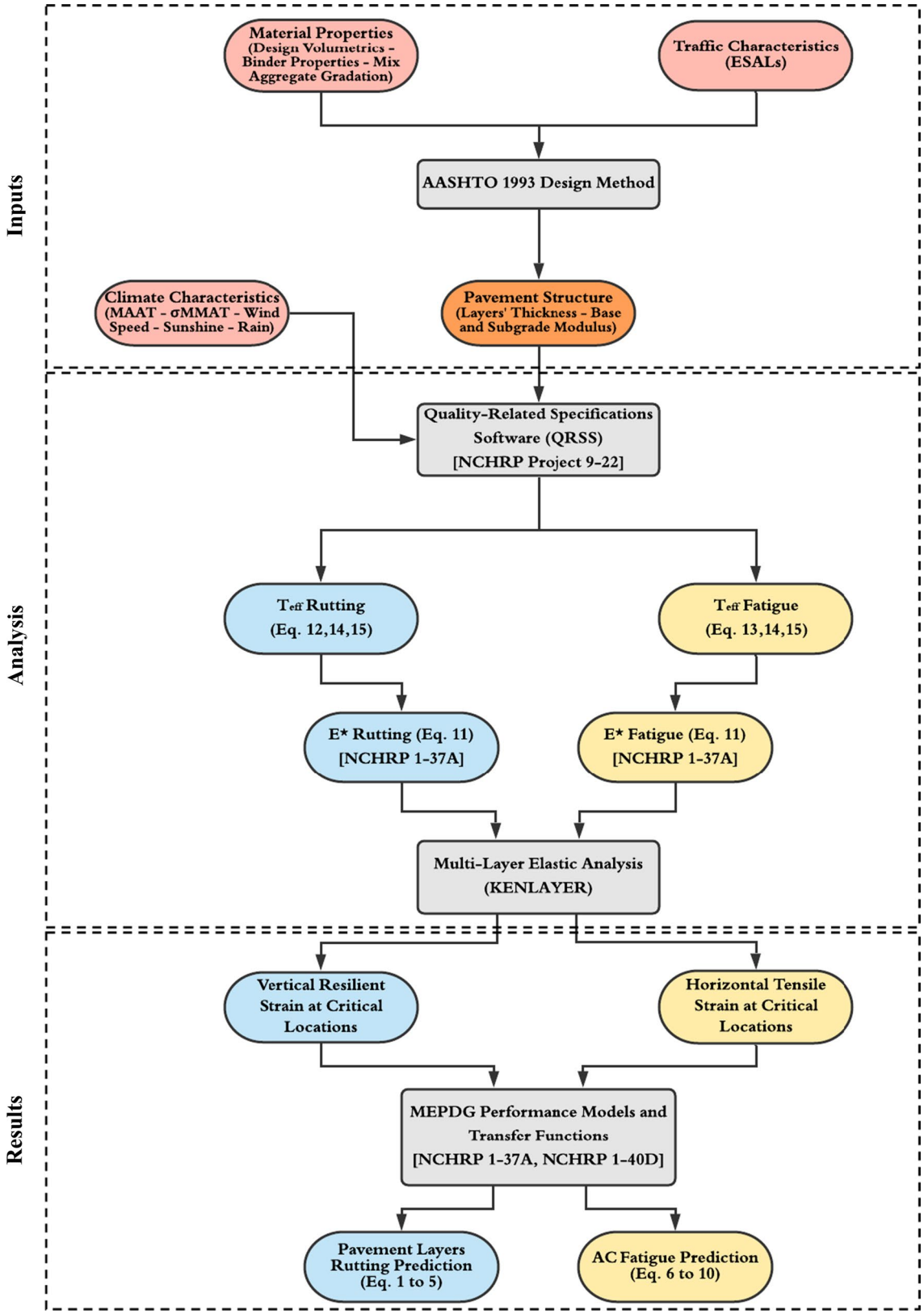

Fig. 1 Flowchart of performance analysis process

properties of the 100% RAP and virgin aggregate materials compared with the Egyptian specifications [49].

A control section (containing 0% RAP) was structurally designed according to the AASHTO 1993 guide [50] for comparing the effect of the base material properties containing different RAP percentages on the field performance over the service life. The laboratory resilient moduli of the base materials, which were used to predict the performance, are available in [24, 51]. The HMA dynamic modulus was predicted by the QRSS. Three different Egyptian climatic conditions of Alexandria, Cairo, and Aswan and two levels of design speeds of 10 and 50 mph (16 and 80 km/h) were chosen for the analysis. Climate data for the three different cities were taken from Elshaeb et al. [52].

Table 6 Input and output parameters for the AASHTO 1993 design method

Input	Design parameters	
	Reliability level (R), %	95
	Combined standard error (S_o)	0.5
	Serviceability	
	Change in serviceability (ΔPSI)	1.5
	Traffic data	
	Total design ESALs (W_{18})	3,000,000
	Design period, years	20
	Asphalt layer	
	Structural layer coefficient (a_1)	0.44
	Base layer	
	Structural layer coefficient (a_2)	0.180
	Drainage coefficient (m)	1.0
	Resilient modulus (M_R), psi	44,465
	Subgrade layer	
	Resilient modulus (M_R), psi	6,000[a]
		15,000[b]
Output	Structural number (SN)	
	SN_1, in.	2.40
	SN_2, in.	5.05[a]
		3.70[b]

SN_1 structural number required above the base layer, SN_2 structural number required above the subgrade layer

[a]Weak subgrade case

[b]Strong subgrade case

The predicted dynamic moduli of the HMA layer |E^*| along with a typical flexible pavement structure were used for the pavement structural analysis model using the Multi-Layer Elastic Analysis (MLEA) software (KENLAYER). The horizontal tensile strain at the bottom of the asphalt layer and the vertical resilient strain at the critical locations within the pavement structure were calculated.

The pavement performance in terms of total pavement rutting and HMA fatigue cracking was predicted using MLEA along with the MEPDG performance models and transfer functions. The same analysis methodology was followed previously by Arisha et al. [53]. Figure 1 outlines the performance analysis process. It should be emphasized that the predicted performance in this research is only valid for comparison purposes because of the simplifications made and also the lack of local calibration of the transfer functions.

Pavement analysis and performance prediction

Control section (0% RAP) was designed for two cases: weak and strong subgrade, following the AASHTO 1993 design method for flexible pavements [50]. The input parameters for the AASHTO 1993 are reliability level (R) = 95%,

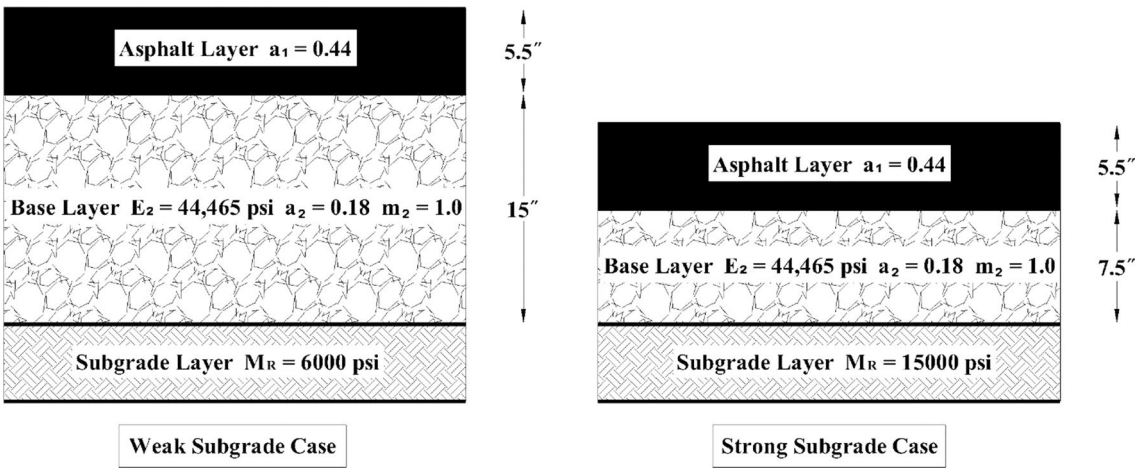

Fig. 2 Pavement structures used for analysis

Table 7 QRSS input parameters for all investigated cases

Traffic input group					
Design speed (mph)					10
					50
Design life (years)					20
Total ESALs					3,000,000
Structure input group					
AC surface thickness (inch)					As illustrated in Fig. 2
Base layer thickness (inch)					
M_r of base layer (psi)					As illustrated in Fig. 2
M_r of subgrade (psi)					
Climate input group					
Climate case	MAAT (°F)	σ_{MMAT} (°F)	Wind speed (mph)	Sunshine (%)	Rain (inch)
Alexandria	71.34	8.33	10.68	88.89	9.15
Cairo	74.42	11.60	6.39	90.09	2.75
Aswan	76.06	12.39	5.36	96.08	0.38

Table 8 Asphalt layer mix inputs [54]

Design volumetric properties inputs	
Air voids, V_a (%)	4.3
Asphalt content by weight, P_b (%)	5.2
Binder characteristics inputs	
A-RTFO[a]	9.599
VTS-RTFO[b]	−3.158
Binder specific gravity, G_b	1.030
Target in situ volumetric properties inputs	
Target in situ air voids (%)	7.0
Aggregate bulk specific gravity, Gs_b	2.610
Mix theoretical bulk specific gravity, G_{mm}	2.447
Mix aggregate gradation inputs	
Percentage passing sieve 1″	100
Percentage passing sieve 3/4″	95
Percentage passing sieve 3/8″	76.5
Percentage passing sieve #4	49.1
Percentage passing sieve #8	45.3
Percentage passing sieve #30	28.9
Percentage passing sieve #50	21.5
Percentage passing sieve #100	12.7
Percentage passing sieve #200	4.8

[a]The intercept of the viscosity–temperature relationship of the rolling thin-film oven (RTFO) aged binder

[b]The viscosity–temperature susceptibility (VTS) which is the slope of the viscosity–temperature relationship of the RTFO aged binder

overall standard deviation (S_o) = 0.50, change in serviceability (ΔPSI) = 1.5 listed in Table 6. A traffic level of three million ESALs and a design life of 20 years were chosen, and the base material moduli were based on the testing results for 0% RAP [24, 51]. The pavement layers' thickness is shown in Fig. 2.

Two levels of design speeds were chosen to evaluate the effect of traffic loading frequency on the effective |*E**| and hence on the predicted pavement performance. The slow speed of 16 km/h (10 mph) simulates the traffic speeds at intersections and toll stations, while the high speed of 80 km/h (50 mph) simulates the typical speed level for rural roads in Egypt. Finally, three different climatic datasets for three Egyptian cities: Alexandria, Cairo, and Aswan, were used to assess the effect of climate on predicted performance. Tables 7 and 8 summarize the inputs for the QRSS for the investigated cases. The HMA properties were taken from Amin [54], and the mix is typically used for wearing surface layers in pavement projects in Egypt. The performance grade (PG) of the binder is compatible with the climatic location.

Dynamic modulus |*E**| prediction

Six QRSS simulation runs were conducted for the different traffic speeds and climate conditions. Table 9 shows the effective frequency, temperature, and AC dynamic modulus for rutting and fatigue. One may surmise from the results that the effective temperature for rutting is higher and hence the effective |*E**| is lower compared to fatigue. Also, as the speed increases, the effective |*E**| also increases due to the viscous nature of the binder. Moreover, |*E**| is lower at the hot climate condition (Aswan) compared to the moderate climate (Alexandria). Finally, the influence of the climate conditions and traffic speed level is more pronounced on the effective |*E**| for rutting as compared to fatigue.

Table 9 QRSS outputs for rutting and fatigue

Speed (mph)	Climate case	Rutting			Fatigue		
		$f_{effective}$ (HZ)	$T_{effective}$ (°F)	E^* (psi)	$f_{effective}$ (HZ)	$T_{effective}$ (°F)	E^* (psi)
10	Alex	7.64	106.71	370,600	8.47	95.02	553,500
	Cairo	10.57	127.63	207,500	8.47	106.27	385,700
	Aswan	10.80	133.15	176,200	8.47	112.96	311,000
50	Alex	34.29	101.66	616,000	42.36	86.63	983,200
	Cairo	36.48	112.53	453,600	42.36	97.88	718,500
	Aswan	37.59	118.01	388,500	42.36	104.57	592,800

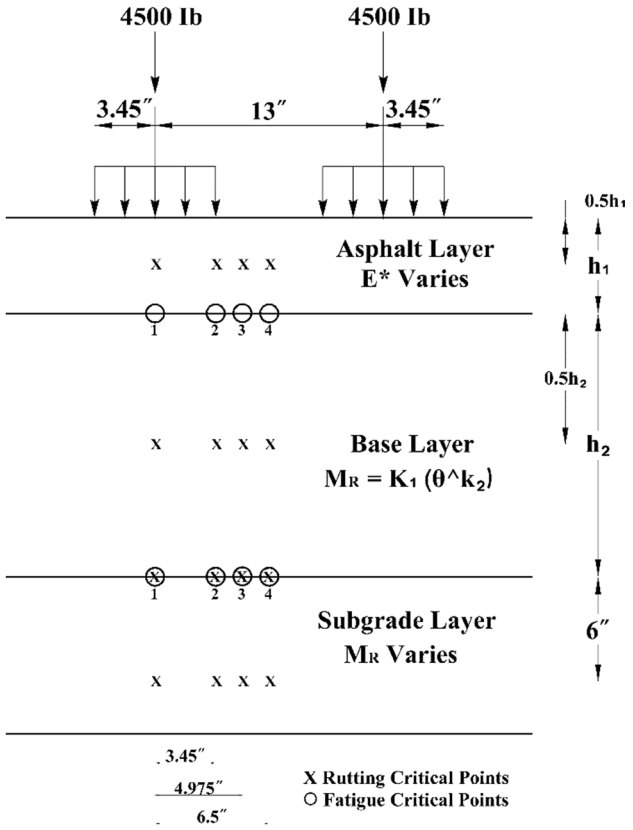

Fig. 3 Cross section used for performance analysis

KENLAYER

KENLAYER is a Multi-Layer Elastic Analysis software designed to analyze flexible pavement stresses and strains. The pavement section used in the simulation runs along with the loading characteristics is demonstrated in Fig. 3. KENLAYER was used for the prediction of vertical resilient strain at different locations within the pavement section [mid-depth of each layer, subgrade surface, and 6 in. (15.24 cm) below subgrade surface]. The vertical resilient strain was used for the calculation of pavement rutting by transfer functions and MEPDG performance models [29]. In addition, the horizontal tensile strain (at the bottom of the AC layer) was also calculated for the determination of fatigue cracking.

The input parameters are material properties and traffic loading. The engineering properties of the base materials are summarized in Table 10. These properties were based on experimental testing results conducted by Mousa et al. [24] and Mousa [51] on different granular base materials blended with different percentages of RAP. A total of 144 runs were conducted.

Traffic repetitions of 3,000,000 18-kips (80-kN) ESALs per the design life, with tire pressure of 120 psi (0.827 MPa) and spacing between the dual tire of 13 in. (33 cm) were applied to the pavement structural sections as displayed in Fig. 3. The nonlinear analysis module was applied for the

Table 10 Material properties for performance analysis [24, 51]

%RAP in base layer	M_r^a, psi (MPa)	Unit weight (pcf)	k_1, psi (MPa)	k_2	Angle of internal friction (φ) (°)
0	44,465.2 (306.8)	140	7651.0 (567.0)	0.48	56
20	54,551.6 (376.3)	137	8734.7 (713.3)	0.50	51
40	64,656.3 (446.1)	137	13,065.8 (779.5)	0.43	53
60	71,210.9 (491.3)	134	16,409.0 (820.1)	0.40	49
80	92,227.3 (636.3)	131	32,368.9 (917.1)	0.28	42
100	105,356.8 (726.9)	124	33,965.3 (1079.2)	0.31	39

[a] M_r values at the anticipated field stresses [$\sigma_1 = 24$ psi (0.166 MPa), $\sigma_3 = 8$ psi (0.055 MPa)]

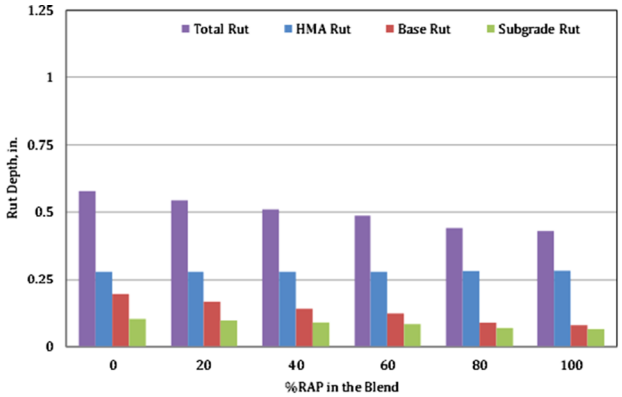

(a) Predicted rut depth for all investigated cases at speed of 10 mph (Alex.).

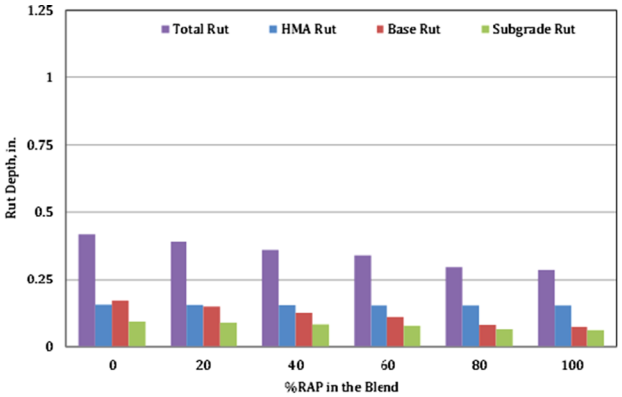

(d) Predicted rut depth for all investigated cases at speed of 50 mph (Alex.).

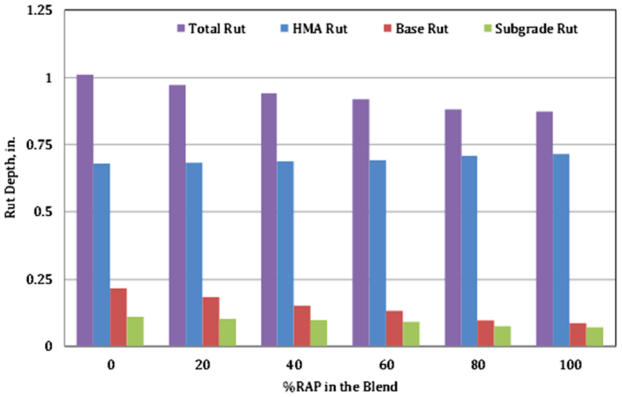

(b) Predicted rut depth for all investigated cases at speed of 10 mph (Cairo).

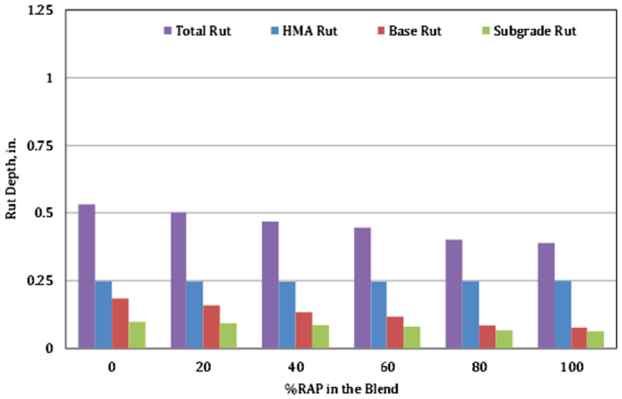

(e) Predicted rut depth for all investigated cases at speed of 50 mph (Cairo).

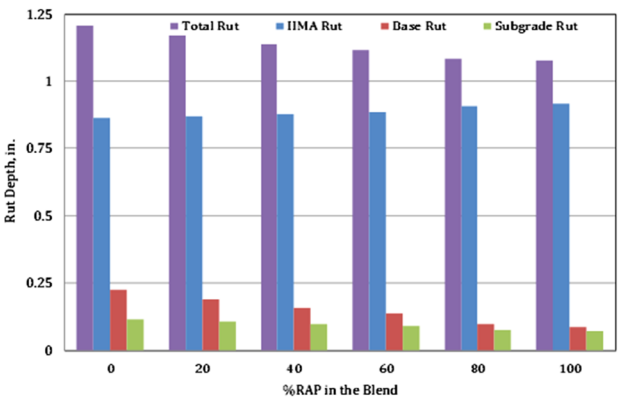

(c) Predicted rut depth for all investigated cases at speed of 10 mph (Aswan).

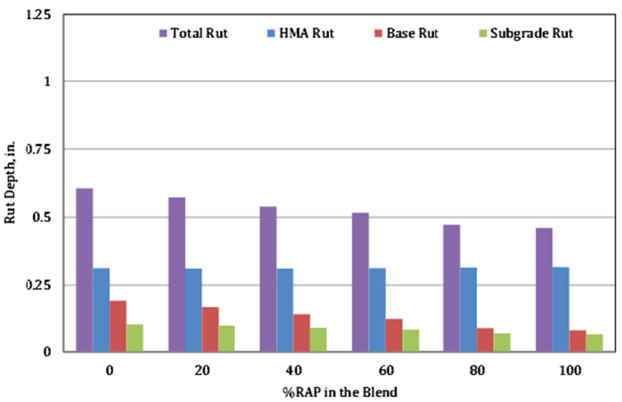

(f) Predicted rut depth for all investigated cases at speed of 50 mph (Aswan).

Fig. 4 Predicted rut depth for the investigated blends (weak subgrade case)

base layer which is based on the $k-\theta$ model ($M_r = K_1\theta^{k_2}$). The pavement system was simulated in the KENLAYER program as three-layered system with the previous traffic characteristic. The resulted values of the horizontal tensile strains and the vertical resilient strains were used as input parameters in the MEPDG performance models and transfer functions for performance predictions, which are presented in the following sections.

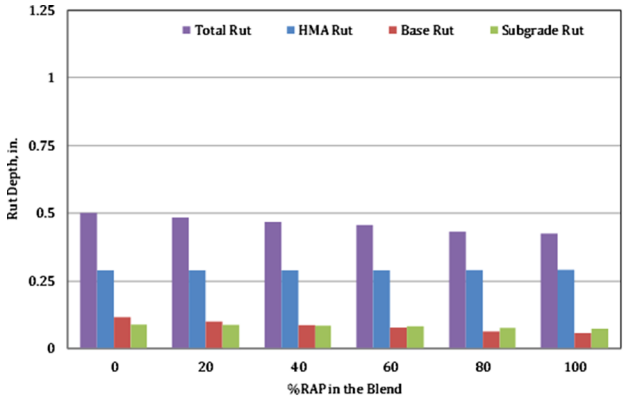

(a) Predicted rut depth for all investigated cases at speed of 10 mph (Alex.).

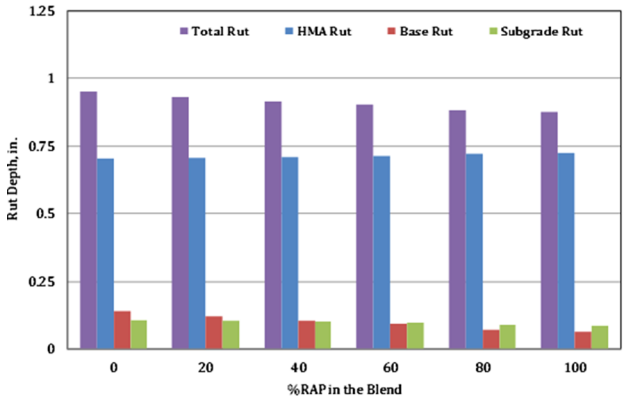

(b) Predicted rut depth for all investigated cases at speed of 10 mph (Cairo).

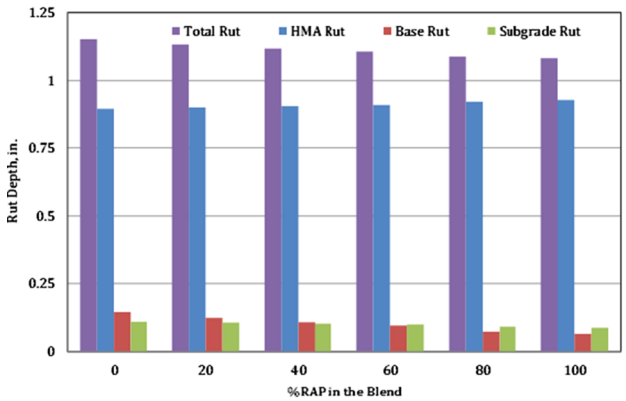

(c) Predicted rut depth for all investigated cases at speed of 10 mph (Aswan).

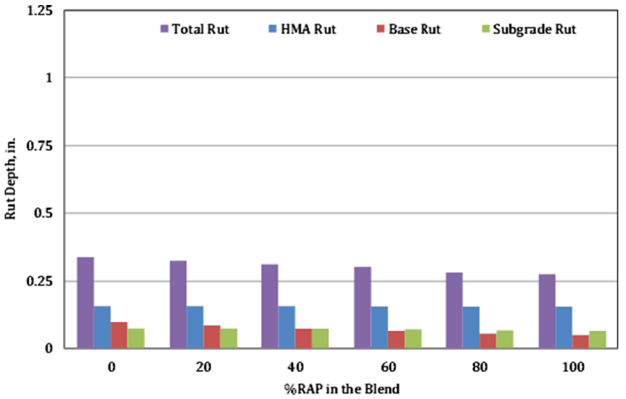

(d) Predicted rut depth for all investigated cases at speed of 50 mph (Alex.).

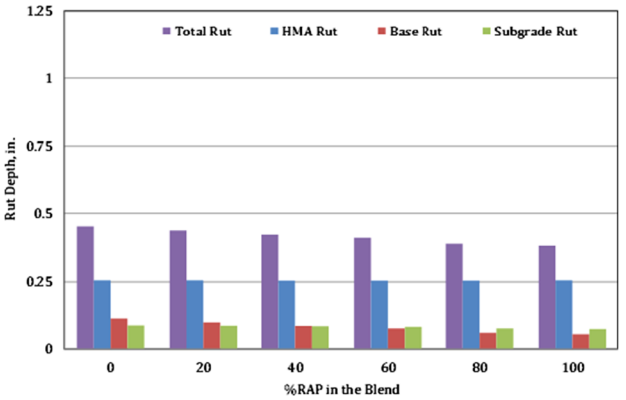

(e) Predicted rut depth for all investigated cases at speed of 50 mph (Cairo).

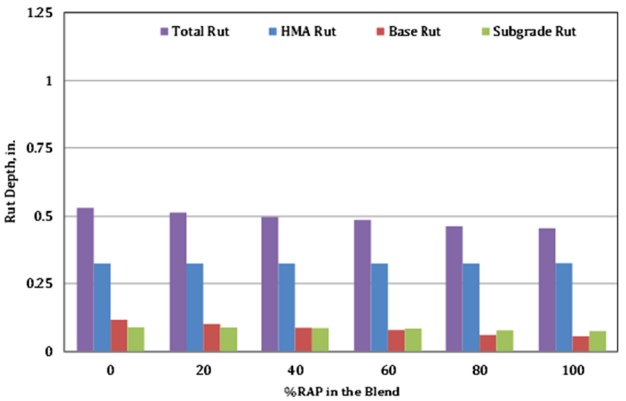

(f) Predicted rut depth for all investigated cases at speed of 50 mph (Aswan).

Fig. 5 Predicted rut depth for investigated blends (strong subgrade case)

Rutting prediction

The predicted rutting against the RAP percentage for all investigated climate cases at the design speed of 10 and 50 mph is presented in Figs. 4 and 5, respectively. It is obvious from the figures that the RAP percentage has a significant effect on the total rutting. The predicted base rut depth was found to increase with the decrease in the RAP

Table 11 Reduction in rut depth due to use RAP in road base: weak-subgrade case

Speed (mph)	Climate case	RAP (%)	Reduction in rut depth (%)			
			HMA	Base	Subgrade	Total depth
10	Alex	0	0.2	0.0	0.0	0.0
		20		14.1	5.8	5.8
		40		27.8	13.0	11.8
		60		36.8	18.8	15.7
		80		54.3	32.5	23.5
		100		58.8	36.6	25.5
	Cairo	0	0.0	0.0	0.0	0.0
		20		15.2	6.8	3.7
		40		29.2	14.4	7.1
		60		38.4	20.3	9.3
		80		55.9	33.6	13.0
		100		60.7	37.8	13.9
	Aswan	0	0.0	0.0	0.0	0.0
		20		15.6	7.0	3.1
		40		29.6	14.6	5.8
		60		38.8	20.5	7.5
		80		56.3	33.6	10.1
		100		61.1	37.8	10.7
50	Alex	0	1.7	0.0	0.0	0.0
		20		13.0	4.5	6.5
		40		26.6	11.0	13.7
		60		35.2	16.3	18.5
		80		52.6	30.0	28.7
		100		56.8	34.0	31.3
	Cairo	0	0.7	0.0	0.0	0.0
		20		13.7	5.3	5.9
		40		27.3	12.3	12.1
		60		36.2	17.9	16.2
		80		53.6	31.7	24.6
		100		58.0	35.8	26.7
	Aswan	0	0.3	0.0	0.0	0.0
		20		14.0	5.7	5.5
		40		27.8	12.9	11.1
		60		36.6	18.6	14.8
		80		54.1	32.3	22.2
		100		58.6	36.4	24.0

amount in the blend for all investigated cases. It should be noted that the rutting of foundation layers (subgrade and granular base layers) does not affect the rutting of the AC layer.

The effect of the climatic condition on rutting prediction is also clear in the figures. As the temperature gets higher (moving from Alexandria to Aswan), the predicted rut depths become higher for all sections at design speed levels of 10 and 50 mph. This observation confirms that the change in asphalt concrete modulus due to the change in temperature has a significant effect on the rutting prediction. Moreover, at high traffic speed level, the values of predicted total rut depths were lower compared to slow traffic speed, which is due to the viscous nature of the asphalt. Thus, the slower the traffic speed (low rate of loading), the larger the rutting in the HMA layer.

Tables 11 and 12 show the reduction in rut depth of each layer due to the use of different RAP amounts in road base for weak- and strong-subgrade soil, respectively. Data show a significant decrease of up to 61% in the base layer rutting and 38% in the subgrade layer rutting when the 100% RAP is used as a base layer compared to the virgin aggregate for

Table 12 Reduction in rut depth due to the use of RAP in road base: strong-subgrade case

Speed (mph)	Climate case	RAP (%)	Reduction in rut depth (%)			
			HMA	Base	Subgrade	Total depth
10	Alex	0	0.1	0.0	0.0	0.0
		20		13.2	1.4	3.4
		40		24.8	3.8	6.6
		60		32.6	6.2	8.9
		80		47.7	13.3	13.5
		100		52.3	16.3	15.1
	Cairo	0	0.0	0.0	0.0	0.0
		20		14.1	2.6	2.1
		40		25.6	5.7	3.8
		60		33.6	8.6	5.0
		80		49.1	16.2	7.2
		100		54.2	19.4	7.9
	Aswan	0	0.0	0.0	0.0	0.0
		20		14.4	2.8	1.7
		40		25.9	6.0	3.0
		60		34.0	9.0	3.9
		80		49.6	16.8	5.6
		100		54.9	20.1	6.1
50	Alex	0	1.4	0.0	0.0	0.0
		20		12.6	0.3	4.0
		40		24.0	1.6	7.9
		60		31.8	3.4	10.7
		80		46.6	9.4	16.7
		100		50.8	12.0	18.6
	Cairo	0	0.4	0.0	0.0	0.0
		20		13.0	1.0	3.5
		40		24.3	2.9	6.8
		60		32.2	5.1	9.2
		80		47.2	11.9	14.1
		100		51.7	14.7	15.6
	Aswan	0	0.1	0.0	0.0	0.0
		20		13.2	1.3	3.2
		40		24.7	3.6	6.1
		60		32.5	6.0	8.2
		80		47.5	13.0	12.6
		100		52.2	15.9	14.0

Aswan at the design speed of 10 mph. The data in Table 11 clearly show that for all practical purposes, the rutting of foundation layers (granular base and subgrade layers) does not affect the rutting of the AC layer. The increase in rut depth reduction is due to the increase in stiffness (resilient modulus) of base layer with the increase in RAP amount in the blend as indicated previously. A maximum decrease of up to 25% in rutting was achieved with the use of 100% RAP relative to 0% RAP (virgin aggregate only) for Alex at a speed of 50 mph. More reduction in total rutting was evident in the case of weak subgrade as compared to the strong subgrade.

Fatigue cracking prediction

Excel sheets were designed for the prediction of fatigue cracking distress using the KENLAYER outputs along with the MEPDG performance models and transfer functions based on the effective temperature calculation for fatigue. Figure 6 presents the predicted fatigue cracking against the RAP percentage for all investigated climate cases at a design speed of 10 and 50 mph. It can be observed from the figures that the fatigue cracking is strongly dependent on the base layer stiffness. As the stiffness of the base layer underneath the AC layer(s) increases (by increasing the RAP

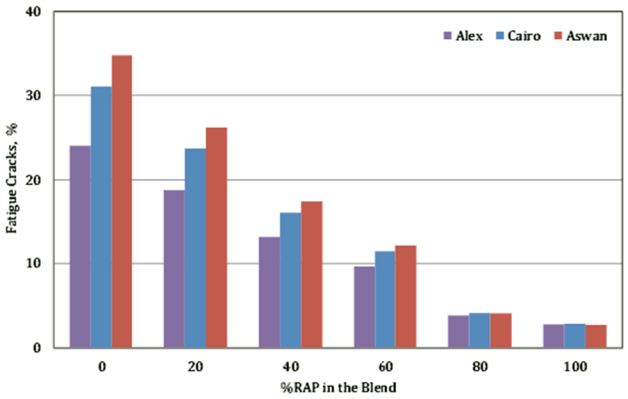

(a) Predicted fatigue cracking at 10 mph design speed for 3 million ESALs – weak subgrade case.

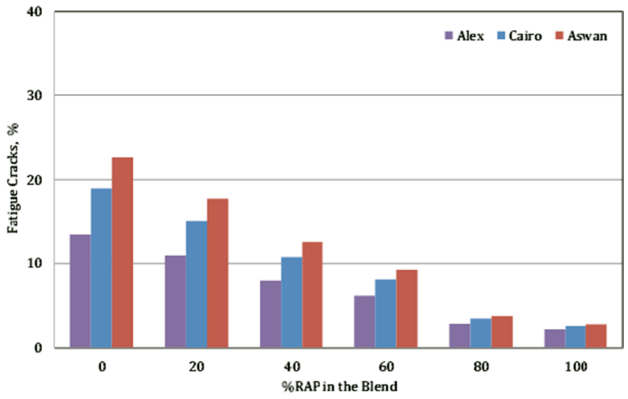

(b) Predicted fatigue cracking at 50 mph design speed for 3 million ESALs – weak subgrade case.

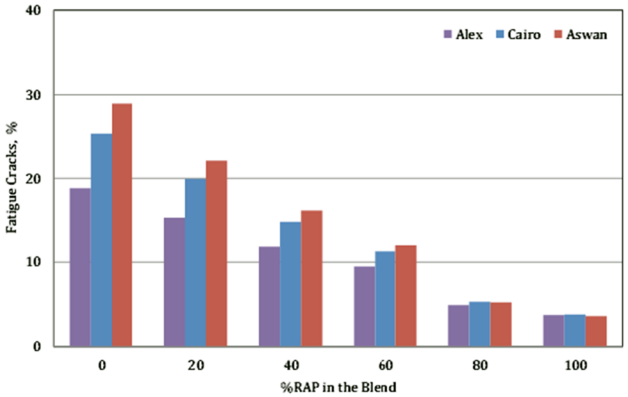

(c) Predicted fatigue cracking at 10 mph design speed for 3 million ESALs – strong subgrade case.

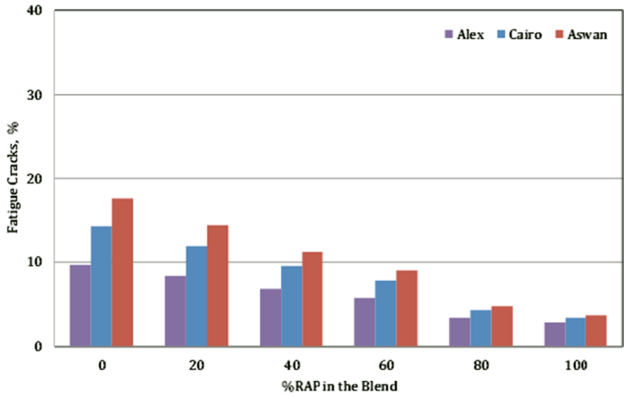

(d) Predicted fatigue cracking at 50 mph design speed for 3 million ESALs – strong subgrade case.

Fig. 6 Predicted fatigue cracking for all investigated cases

amount in the blend), the tensile strain at the bottom of the HMA layer decreases, and consequently, fatigue cracking decreases. Alam et al. [5] reported the same observation for the decrease in fatigue cracking with the increase in RAP amount. Also as seen from the figure, the fatigue cracking for strong-subgrade cases is lower than weak-subgrade soil at the same speed and climate condition. The reason for this is that as the subgrade stiffness increases, the tensile strain (at the bottom of the HMA layer) decreases, and hence fatigue cracking decreases.

The effect of the climatic condition on fatigue cracking is also obvious in figures. In general, as the temperature gets higher (moving from Alexandria to Aswan), the fatigue cracking gets higher. The significance of climatic conditions on fatigue cracking agrees with the findings of Ezzat et al. [55], Tarbay et al. [56] and Azam et al. [57] studies.

The effect of traffic speed is presented in the same figure; at slow speed, the predicted fatigue cracking values were higher compared to fast speed due to the viscous behavior of the asphalt material. The significance of the selected climates on the values of the predicted fatigue cracking is minor as the Egyptian climate is mostly hot and moderate and.

Table 13 summarizes the reduction in fatigue cracking for the different percentages of RAP in road base for weak- and strong-subgrade soil. A maximum decrease of up to 92% and 88% was observed in the fatigue cracking when the 100% RAP was used as a base layer compared to the virgin aggregate for Aswan at the design speed of 10 mph for weak and strong subgrade, respectively. The increase in fatigue cracking reduction is due to the increase in resilient modulus of the base layer material with the increase in RAP amount as indicated previously.

Table 13 Reduction in fatigue cracking due to the use of RAP in road base for all investigated cases

Speed (mph)	Climate case	RAP (%)	Reduction in fatigue cracking (%)	
			Weak subgrade	Strong subgrade
10	Alex	0	0.0	0.0
		20	21.8	18.5
		40	45.4	36.6
		60	59.8	49.8
		80	83.9	74.0
		100	88.3	80.1
	Cairo	0	0.0	0.0
		20	23.7	21.1
		40	48.1	41.1
		60	63.1	54.9
		80	86.7	79.0
		100	90.8	84.9
	Aswan	0	0.0	0.0
		20	24.8	23.3
		40	49.8	43.8
		60	65.1	58.0
		80	88.2	81.8
		100	92.2	87.5
50	Alex	0	0.0	0.0
		20	18.3	13.5
		40	40.5	29.4
		60	54.1	40.6
		80	78.8	64.5
		100	83.4	70.7
	Cairo	0	0.0	0.0
		20	20.3	16.4
		40	43.4	33.5
		60	57.4	45.7
		80	81.8	69.9
		100	86.3	76.1
	Aswan	0	0.0	0.0
		20	21.5	18.0
		40	44.7	35.8
		60	59.1	48.8
		80	83.4	72.9
		100	87.8	79.1

Conclusions

This study combined three powerful tools: MLEA, transfer functions, and MEPDG performance models, and the QRSS software in a simplified methodology to predict the pavements performance constructed using RAP/virgin aggregate blends as base course material for road construction in Egypt. Based on the laboratory and performance prediction results and analyses, the following conclusions can be found:

1. RAP blends showed superior/comparable performance compared to virgin aggregates.
2. The effects of rate of loading (vehicle speed), climatic conditions and subgrade strength were significant on both fatigue cracking of the AC layer and rutting of asphalt, base, and subgrade.
3. The state of stress at the base layer had a significant effect on the modulus of the layer and consequently on the pavement performance. Further laboratory testing is required to determine the dynamic modulus of the HMA, since the prediction of pavement performance is mainly based on the predicted values of $|E^*|$.

Acknowledgements The authors are forever grateful to Dr. Mohamed El-Shabrawy, Late Professor of Highway, Traffic, and Transportation Engineering, Public Works Engineering Department, Faculty of Engineering, Mansoura University, for his guidance, insights, unconditional support, valuable feedback, and encouragement at the beginning of this research.

References

1. Kim YR, Jadoun FM, Hou T, Muthadi (2011) Local calibration of the MEPDG for flexible pavement design. Final report Raleigh, North Carolina State University and NC Department of Transportation, Research and Analysis Group, NC
2. Azam AM, Cameron DA (2013) Laboratory evaluation of recycled concrete aggregate and recycled clay masonry blends in pavement applications. J Adv Civil Eng Mater ASTM 2(1):328–346
3. Bolden J, Abu-Lebdeh T, Fini E (2013) Utilization of recycled and waste materials in various construction applications. Am J Environ Sci 9(1):14–24
4. El-Badawy SM, Gabr AR, Abdel Hakim RT (2018) Recycled materials and by-products for pavement construction. In: Martínez LMT, Kharissova OV, Kharisov BI (eds) Handbook of ecomaterials. Springer, New York, pp 1–22
5. Alam TB, Abdelrahman M, Schram SA (2010) Laboratory characterisation of recycled asphalt pavement as a base layer. Int J Pavement Eng 11(2):123–131
6. Sayed SM, Pulsifer JM, Jackson NM (2011) UNRAP: are we ready for it? J Mater Civ Eng 23(2):188–196
7. Wu M (2011) Evaluation of high percentage recycled asphalt pavement as base course materials. Master's thesis, Washington State University, DC, USA
8. Dong Q, Huang B (2014) Laboratory evaluation on resilient modulus and rate dependencies of RAP used as unbound base material. J Mater Civ Eng 26(2):379–383
9. Kolay PK, Singh P (2016) Resilient modulus of a blended mixture of recycled asphalt pavement and natural aggregate as road pavement base material. In: ASCE Geo-Chicago 2016, sustainability, energy, and the geoenvironment, pp 677–686
10. Sayed SM, Pulsifer J, Schmitt R (1993) Construction and performance of shoulders using UNRAP base. Journal of Materials in Civil Engineering 5(3):321–338

11. Garg N, Thompson MR (1996) Lincoln avenue reclaimed asphalt pavement base project. Transp Res Rec J Transp Res Board 1547:89–95
12. Papp WJ, Maher MH, Bennert H, Gucunski N (1998) Behavior of construction and demolition debris in base and subbase applications. Geotech Spec Publ 79:122–135
13. Taha R, Ali G, Basma A, Al-Turk O (1999) Evaluation of reclaimed asphalt pavement aggregate in road bases and subbases. Transp Res Rec J Transp Res Board 1652:264–269
14. MacGregor JAC, Highter WH, DeGroot DJ (1999) Structural numbers for reclaimed asphalt pavement base and subbase course mixes. Transp Res Rec J Transp Res Board 1687:22–28
15. Bejarano MO (2001) Evaluation of recycled asphalt concrete materials as aggregate base. Technical Memorandum TMUCB-PRC-2001-4. California Department of Transportation, District 2 Materials Branch, Sacramento, CA
16. Cosentino PJ, Kalajian E, Shieh CS, Mathurin WJ, Gomez FA, Cleary ED, Treeratrakoon A (2003) Developing specifications for using recycled asphalt pavement as base, subbase or general fill materials, Phase II. Report no. FL/DOT/RMC/06650-7754, Civil Engineering Department, Florida Institute of Technology, State Materials Office, Florida Department of Transportation, Gainesville, FL
17. Bennert T, Maher A (2005) The development of a performance specification for granular base and subbase material. Publication FHWA-NJ-05-003. FHWA, US Department of Transportation, Washington, DC
18. Trzebiatowski BD, Benson CH (2005) Saturated hydraulic conductivity of compacted recycled asphalt pavement. Geotechnical Testing Journal 28(5):1–6
19. Guthrie SW, Cooley D, Eggett DL (2007) Effects of reclaimed asphalt pavement on mechanical properties of base materials. Transp Res Rec Transp Res Board 2005:44–52
20. Gupta SC, Kang DH, Ranaivosoon A (2009) Hydraulic and mechanical properties of recycled materials. Report 2009-32, Minnesota Department of Transportation, University of Minnesota, USA
21. Locander R (2009) Analysis of using reclaimed asphalt pavement (RAP) as a base course material. Report No. CDOT-2009-5, Colorado Department of Transportation—Research, Denver
22. Luo C (2014) High performance granular base and subbase materials incorporating reclaimed asphalt concrete pavement. Master's thesis, McMaster University, Hamilton, Ontario
23. Stolle DFE, Guo P, Emery JJ (2014) Mechanical properties of reclaimed asphalt pavement: natural aggregate blends for granular base. Can J Civ Eng 41(6):493–499
24. Mousa E (2017) Performance of RAP as base course for paved and unpaved roads in Egypt. Master's thesis, Mansoura University, Egypt
25. Alotaibi A, El-Badawy S, Elshabrawy MA (2011) Asphalt pavement recycling as a subbase layer for the Egyptian roads. J Environ Sci 40(1):1–13
26. Thakur JK, Han J (2015) Recent development of recycled asphalt pavement (RAP) bases treated for roadway applications. Transp Infrastruct Geotechnol 2(2):68–86
27. Saride S, George AM, Avirneni D, Basha BM (2017) Sustainable design of Indian rural roads with reclaimed asphalt materials. In: Sustainability issues in civil engineering. Springer, Singapore, pp 73–90
28. Schwartz CW, Li R, Ceylan H, Kim S, Gopalakrishnan K (2013) Global sensitivity analysis of mechanistic-empirical performance predictions for flexible pavements. Transp Res Rec Transp Res Board 2368:12–23
29. Applied Research Associates (ARA) (2008) Mechanistic-empirical pavement design guide: a manual of practice. American Association of State Highway and Transportation Officials, Washington
30. NCHRP (2011) Beta testing and validation of HMA PRS. Project no. NCHRP 9-22, Fugro Consultants Inc., Arizona State University, Phoenix, Arizona, USA
31. Salim R (2019) Asphalt binder parameters and their relationship to the linear viscoelastic and failure properties of asphalt mixtures. PhD thesis, Arizona State University
32. Awed A, El-Badawy S, Bayomy F, Santi M (2011) Influence of the MEPDG binder characterization input level on the predicted dynamic modulus for Idaho asphalt concrete mixtures. In: Proceedings of the transportation research board 90th annual meeting, Washington DC, USA
33. El-Badawy S, Bayomy F, Awed A (2012) Performance of MEPDG dynamic modulus predictive models for asphalt concrete mixtures: local calibration for Idaho. J Mater Civ Eng 24(11):1412–1421
34. Khattab AM, El-Badawy SM, Elmwafi M (2014) Evaluation of Witczak E* predictive models for the implementation of AASHTOWare-pavement ME design in the Kingdom of Saudi Arabia. Constr Build Mater 64:360–369
35. Khattab AM, El-Badawy SM, Al Hazmi AA, Elmwafi M (2015) Comparing Witczak NCHRP 1-40D with Hirsh E* predictive models for Kingdom of Saudi Arabia asphalt mixtures. In: 3rd Middle East Society of asphalt technologists (MESAT) conference American University in Dubai, UAE
36. Ali Y, Irfan M, Ahmed S, Khanzada S, Mahmood T (2015) Investigation of factors affecting dynamic modulus and phase angle of various asphalt concrete mixtures. Mater Struct 49(3):857–868
37. Georgouli K, Plati C, Loizos A (2016) Assessment of dynamic modulus prediction models in fatigue cracking estimation. Mater Struct 49(12):5007–5019
38. Georgouli K, Loizos A, Plati C (2016) Calibration of dynamic modulus predictive model. Constr Build Mater 102:65–75
39. El-Badawy S, Abd El-Hakim R, Awed A (2018) Comparing artificial neural networks with regression models for hot-mix asphalt dynamic modulus prediction. J Mater Civ Eng 30(7):04018128
40. Moulthrop J, Witczak M (2011) A performance-related specification for hot-mixed asphalt. NCHRP report 704, Transportation Research Board, Washington, DC
41. El-Badawy S, Jeong M, El-Basyouny M (2009) Methodology to predict alligator fatigue cracking distress based on AC dynamic modulus. Transp Res Rec J Transp Res Board 2095:115–124
42. AASHTO T 164-97 (2002) Quantitative extraction of bitumen from bituminous paving mixtures. American Association of State Highway and Transportation Officials, Washington
43. AASHTO T 27-99 (2012) Sieve analysis of fine and coarse aggregates. American Association of State Highway and Transportation Officials, Washington
44. AASHTO T 96-99 (2012) Resistance to degradation of small-size coarse aggregate by abrasion and impact in the Los Angeles machine. American Association of State Highway and Transportation Officials, Washington
45. AASHTO T 89-96 (2014) Determining the liquid limit of soils. American Association of State Highway and Transportation Officials, Washington
46. AASHTO T 90-00 (2015) Determining the plastic limit and plasticity index of soils. American Association of State Highway and Transportation Officials, Washington
47. AASHTO M 145-91 (2012) Classification of soils and soil-aggregate mixtures for highway construction purposes. American Association of State Highway and Transportation Officials, Washington
48. AASHTO T 180-97 (2012) Moisture-density relations of soils using a 4.54-kg (10-ib) rammer and a 457-mm (18-in.) drop. American Association of State Highway and Transportation Officials, Washington
49. Egyptian code of practice (ECP-104) (2018) Egyptian code of practice for urban and rural Roads. Housing and Building National Central Research, Cairo

50. American Association of State Highway and Transportation Officials (AASHTO) (1993) AASHTO guide for design of pavement structures, Washington
51. Mousa E, Azam A, El-Shabrawy M, El-Badawy SM (2017) Laboratory characterization of reclaimed asphalt pavement for road construction in Egypt. Can J Civ Eng 44(6):417–425
52. Elshaeb M, El-Badawy S, Shawaly A (2014) Development and impact of the Egyptian climatic conditions on flexible pavement performance. Am J Civ Eng Archit 2(3):115–121
53. Arisha AM, Gabr AR, El-Badawy SM, Shwally SA (2018) Performance evaluation of construction and demolition waste materials for pavement construction in Egypt. J Mater Civ Eng 30(2):1–14
54. Amin I (2016) Laboratory evaluation of asphalt binder modified with carbon nanotubes. Master's thesis, Mansoura University, Egypt
55. Ezzat H, El-Badawy S, Gabr A, Zaki S, Breakah T (2020) Predicted performance of hot mix asphalt modified with nano-montmorillonite and nanosilicon dioxide based on Egyptian conditions. Int J Pavement Eng. https://doi.org/10.1080/10298436.2018.1502437
56. Tarbay EW, Azam AM, El-Badway S (2019) Waste materials and by-products as mineral fillers in asphalt mixtures. Innov Infrastruct Solut J 4(1):1–13
57. Azam AM, El-Badway S, Alabasee R (2019) Evaluation of asphalt mixtures modified with polymer and wax. Innov Infrastruct Solut 4(43):1–12